BROOKHAVEN
NATIONAL LABORATORY

BNL-77678-2007-CP

CdZnTe room-temperature semiconductor gamma-ray detector for national-security applications

G. S. Camarda, A. E. Bolotnikov, *Member, IEEE*, Y. Cui, *Member, IEEE*, A. Hossain, K. T. Kohman, and R. B. James, *Fellow, IEEE*

Brookhaven National Laboratory
Upton, NY 11793

Third Annual IEEE Long Island Systems
Applications and Technology (LISAT) Conference
Institute for Research & Technology Transfer, Farmingdale State University
Farmingdale, NY
May, 4, 2007

Nonproliferation and National Security Department
Detector Development and Testing Division

Brookhaven National Laboratory
P.O. Box 5000
Upton, NY 11973-5000
www.bnl.gov

DISCLAIMER

CdZnTe room-temperature semiconductor gamma-ray detector for national-security applications

G. S. Camarda, A. E. Bolotnikov, *Member, IEEE*, Y. Cui, *Member, IEEE*, A. Hossain, K. T. Kohman, and R. B. James, *Fellow, IEEE*

***Abstract*—One important mission of the Department of Energy's National Nuclear Security Administration is to develop reliable gamma-ray detectors to meet the widespread needs of users for effective techniques to detect and identify special nuclear- and radioactive-materials. Accordingly, the Nonproliferation and National Security Department at Brookhaven National Laboratory was tasked to evaluate existing technology and to develop improved room-temperature detectors based on semiconductors, such as CdZnTe (CZT). Our research covers two important areas: Improving the quality of CZT material, and exploring new CZT-based gamma-ray detectors. In this paper, we report on our recent findings from the material characterization and tests of actual CZT devices fabricated in our laboratory and from materials/detectors supplied by different commercial vendors. In particular, we emphasize the critical role of secondary phases in the current CZT material and issues in fabricating the CZT detectors, both of which affect their performance.**

***Index Terms*—CdZnTe, radiation detectors, Te inclusions**

I. Introduction

LARGE volume CdZnTe (CZT) semiconductor offers several advantages as a detecting medium for x- and gamma-rays and has being considered by the Department of Energy and other agencies for detection of special nuclear and radioactive materials [1]. However, there are several obstacles that still limit the wide use of this promising technology [2-5]. Recently, evidences have grown that Te inclusions (usually present in CZT material) are the main cause affecting the performance of thick (long-drift) CZT detectors, thereby limiting the size and efficiency of such detectors available to users [6-9]. According to Rudolph [10], Te inclusions represent one type of several non-stoichiometric related defects normally formed during the melt growth of CZT. The other three are intrinsic point defects (vacancies, interstitials and anti-sites), which alter the bulk conductivity, dislocations, and Te precipitates both of which form during the cooling process as a result of nucleation of native defects. High-resolution transmission electron microscopy revealed that the Te precipitates are 10-50 nm [10], while the typical diameters of Te inclusions are 1-2 μm, although sizes up to 100 um are observed in high-pressure and vertical Bridgman grown CZT [10]. Thus, the particles usually seen with IR microscopy (where optical resolution is limited to 1 μm) are attributed to the Te inclusions. In CZT material their concentrations may exceed 10^7 cm^{-3}, but this is still several orders-of-magnitude smaller than that of the Te precipitates [10].

Recently, we employed a highly collimated X-ray beam at the National Synchrotron Light Source (NSLS) at Brookhaven National Lab (BNL) to measure directly the charge trapped by individual inclusions in CZT samples [6,7]. These results provided clear evidence for the long-discussed hypothesis of the cumulative effect of Te inclusions in thick CZT detectors. Modeling [8,9] of the electron-cloud transport through CZT material containing Te inclusions showed that their cumulative effect can explain the degradation of energy resolution observed in thick CZT detectors, and further, that the magnitude of the effect strongly depends on their size and concentration. Moreover, simulations predicted that inclusions of less than ~1 um diameter essentially behave as ordinary traps associated with point defects (native or impurities) in the material. Such defects trap the electrons but do not introduce fluctuations in the collected charge signals, allowing for correction of the total charge loss using a depth-sensing technique. Interestingly, Te precipitates also may behave as point defects, and since their concentration in as-grown material can be high, they might control the effective mobility-lifetime product for both holes and electrons. Thus, to maximize the performance of CZT detectors, it is important to establish the limits of the sizes and concentration of the inclusions as a function of the device's thicknesses.

In the course of our project to develop an array of Frisch-ring CZT detectors [11,12], we fabricated and tested the spectral responses of ~20 bar-shaped CZT samples ranging from 5 to 15 mm thick. Theoretically, the geometry of these samples so configured should provide a spectral response with

Manuscript received February 15, 2007. This work was supported by U.S. Department of Energy, Office of Nonproliferation Research and Engineering, NA-22. The manuscript has been authored by Brookhaven Science Associates, LLC under Contract No. DE-AC02-98CH1-886 with the U.S. Department of Energy.

A. E. Bolotnikov, G. S. Camarda, A. Hossain, Y. Cui, and R. B. James are with Brookhaven National Laboratory, Upton, NY 11793 USA (phone: 631-344-8014; e-mail: bolotnik@bnl.gov).

K.T. Kohman is with Kansas State University, Manhattan, KS 66506 USA.

energy resolution of 0.7-1.5% at 662 keV depending on the device's length and the electron mobility-lifetime product. However, the performance of many samples was much worse than expected. Visualization of these CZT samples via an IR microscope invariably revealed a high concentration of Te inclusions that, we believe, cause large fluctuations of the collected charge. These qualitative observations stimulated our further investigations, which are described in this article.

Here, we report on quantitative measurements of the correlation between the size and concentrations of Te inclusions and the devices' responses. The sizes and concentrations of the Te inclusions were determined with an automated IR imaging system developed at BNL to screen semiconductor devices. The results predict the extent to which Te inclusions can be tolerated in CZT crystals.

II. Experimental

We used Frisch-ring detectors to measure the fluctuations of the collected charge caused by Te inclusions and enhanced by the long drift distances of the electron clouds. The detectors fabricated from high-quality single-crystal CZT (containing no twins, grains or inclusions >50 μm) with two planar contacts were supplied by several vendors employing different growth techniques. Each crystal first was screened with our IR microscopy system to obtain the information about the sizes and concentrations of Te inclusions, and then configured as Frisch-ring detectors [11,12] for measurements with gamma rays. The detectors' thicknesses were between 5-15 mm, typically with a geometrical cross-section of ~5x5 mm^2. During measurements, the detector was placed inside a device holder connected to a box containing the eV-5092 preamplifier that provided electronic noise of 3-4 keV FWHM (~0.5% at 662 keV). The shielding electrode (the Frisch-ring) was connected to the cathode and kept at zero potential, while the positive voltage was applied to the anode via a pogo-pin connector. Depending on the device's thickness, we applied 1500-3000 V biases to achieve the optimal device performance. The detectors were irradiated with gamma rays from a ^{137}Cs source located near the cathode. The data-acquisition system included a spectroscopy amplifier, MCA card, and standard NIM electronics.

Using our automated IR imaging system developed for accurately screening defects in large-volume CZT crystals, we evaluated the sizes and concentrations of Te inclusions in the tested samples. The system, shown in Fig. 1, includes a fiber-optic light source coupled with a wide-beam condenser illuminating the samples, a large field-of-view (FOV) microscope objective, a CCD camera, and an in-line optical assembly system mounted in line with motorized X-Y-Z translation stages. The CCD camera has a sensor area of 7.8 x 10.6 mm^2 and provides 2208x3000 pixels, each of 3.5 um. The camera is connected to the PC by firewire cable and controlled, as are the actuators, by specifically written C++ software. The long working-distance objectives had magnifications from 2x to 20x; the typical system's FOV was 5.3x3.8 mm^2 at the 2x magnification.

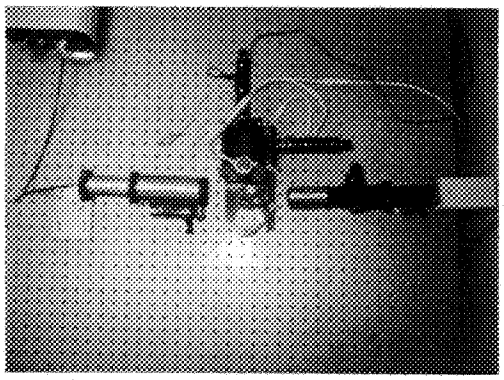

Fig. 1. A view (from the top) of the automated IR imaging system which includes a fiber-optic light source coupled with a wide-beam condenser illuminating the samples, a large field-of-view microscope objective, a CCD camera, and motorized translation stages.

The CZT samples were placed on the translation stages. We eliminated non-uniformities due to the illuminating light's intensity and special variations of the CCD camera's response by properly flat-field calibrating the system before taking the measurements. The system can perform a one-, two-, or three-dimensional raster scan of a CZT crystal. At each X-Y-Z position, an image of the area is taken and saved, and then the translation stages move the sample to the next position where this is repeated, and so on. The images were saved as monochrome high-resolution jpeg files, with 8-bit dynamic range.

The step size of the raster scan depends on the FOV adopted. The system was principally utilized to measure the size and the concentration of Te inclusions per cm^3 of CZT crystals grown by different techniques. We describe below the iterative algorithm developed to locate Te inclusions in the images and identify their shapes and sizes. To determine the concentration of Te inclusions per cm^3, after choosing a particular X-Y area, we took a one-dimensional scan in the Z direction (in depth). For example, considering a 5 mm-thick CZT sample, and using a 50 μm Z-scan step, 100 different images were acquired. Ideally, these 100 IR micrographs can be stitched together in the Z direction to form a known volume of CZT, and then the concentration of Te inclusions can be obtained by counting the number of inclusions in the volume analyzed.

For each CZT sample, the size distribution of Te inclusions and their concentration were evaluated by averaging over five different measurements taken at five different locations over the crystal's length from two perpendicular directions. When scanning in the z direction, the step size for the scan depends on the microscope objective's depth of focus (DOF). For example, using a 5x magnification, the associated DOF was 14 μm. After the scan in the Z direction, ~100 images were ready for analysis. We describe the iterative algorithm developed to locate Te inclusions in the images and identify their shapes and sizes below.

Image processing is an important part of our experimental procedure. CZT crystals are transparent to the infrared light; however, using long wavelength light limits the feature's minimum size to ~1 μm. In the IR images, Te inclusions larger than 5 μm are seen as relatively sharp objects with apparent

shapes depending on crystal's orientation and the illumination. Usually, Te inclusions have triangular or diamond-like shapes. In 3D images (pixel-intensity distributions), such inclusions are represented by three-dimensional surfaces, in some cases, comprised of several Gaussian-like functions. Small sized inclusions, below 3 μm, typically appear as blurred objects with surrounding artificial haloes. In a 3D image, such inclusions are represented by surfaces with two-dimensional Gaussian functions.

We used the IDL (Interactive Data Language) programming environment that is especially well suited for image manipulation and processing and with powerful input/output facilities, along with variety of e libraries for statistical analysis and plotting the results. The imaging setup allowed us to acquire stacks of images, each focused at different depth of the crystal. Table 1 lists the typical parameters of the microscope. It shows that at high magnifications, larger than x2, the depth of focus is comparable to the expected size of the precipitate ~10 μm. In principle, with such an apparatus, the crystal's volume can be "scanned" or "sliced" completely.

TABLE I
PARAMETERS OF THE MICROSCOPE OPTICS USED FOR THE CZT ANALYSIS

Magnification	2x	5x	10x	20x
Numerical Aperture	0.055	0.14	0.28	0.42
Working Distance, mm	34.0	34.0	33.5	20.0
Focal Length, mm	100	40	20	10
Resolving Power, um	5.0	2.0	1.0	0.7
Depth of Focus, um	91.0	14.0	3.5	1.6

The first step in image processing was to invert the original images so the features representing inclusions were regions of high intensity (peaks). To improve image recognition background, filtering is needed to suppress the contributions from image noise or image defects. We used several techniques for this, from simple threshold application to band-pass filtering. Both techniques equally generate good-quality images with uniform illumination and few noise artifacts. A real-space, band-pass filter suppresses pixel noise and slow-scale image variations while retaining information on characteristic size; this is beneficial for images with non-uniform illumination or multiple surface-related defects (such as scratches). Because the illumination of the focal plane at which images are taken can vary from sample to sample and even from image to image, the threshold values must be iteratively adjusted to optimize the quality of the determination of the precipitates' parameters.

After suppressing the background, we could begin searching for features and determining their properties. We utilized the following algorithm for peaks localization: First, we identified the positions of all the local maxima in the image (defined in a circular neighborhood with some given diameter), then placed a circular mask of the same size around each maxima, and calculated the X and Y positions of centroids, the total brightness of all the pixels, and the diameters of the pixels within that mask. If the initial local maximum was more than 0.5 pixels from the centroid, the mask was moved and the data re-calculated. This manipulation is useful for noisy data. If the image noise was small and the features more than about 5 pixels across, then we expected the resulting X and Y values to have errors of the order of ~0.5 pixels for reasonably noise-free images. For the band-pass filter and feature search, we used Crocker and Grier's algorithms [13]. The output of the feature-determination routine is an array which contains the following parameters: XY-coordinates of the found feature, its integrated brightness, and its diameter evaluated as full-width-at-half-maximum of peaks. Subsequent analysis and identification of found features as inclusions is based on these parameters. Fig. 2 gives an example of an identified triangular-shape inclusion, labeled with its parameters. Faint out-of-focus features also are clearly visible. As depicted in this picture, images may contain different kinds of features, noise, proper inclusions, and faint outlines of out-of-focus inclusions that do not "belong" to the current slice of the sample.

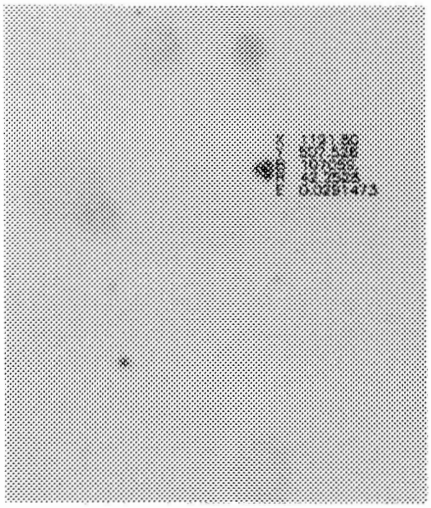

Fig. 2. Example of an identified triangular-shape inclusion, labeled with its parameters with the faint out-of-focus features in the background.

To exclude the out-of-focus features, we use several criteria - one of which is correlations between inclusions diameters and their brightness (Fig. 3). As illustrated in Fig. 3, the radius versus brightness distribution has two distinguishable areas of high dots concentration corresponding to two different classes of objects. Large objects, with low brightness, are identified as out-of-focus inclusions. Objects smaller in size but with higher brightness are identified with true, in-focus inclusions. Visual inspection of the images confirmed this hypothesis. Visual inspection of the images confirmed this hypothesis. We concluded that integrated brightness proved to be the most discriminating variable, allowing us to reject out-of-focus features and select in-focus inclusions. Typically, after background subtraction and with a relaxed cut on brightness, the program identified up to several hundred features. After adjusting the cut on brightness, this number fell to less than twenty, with the exact number depending on the image's magnification and quality. Such visual inspections before and after processing the images led

us to conclude that this procedure can yield an accuracy of determination of in-plane inclusions of better than 3%.

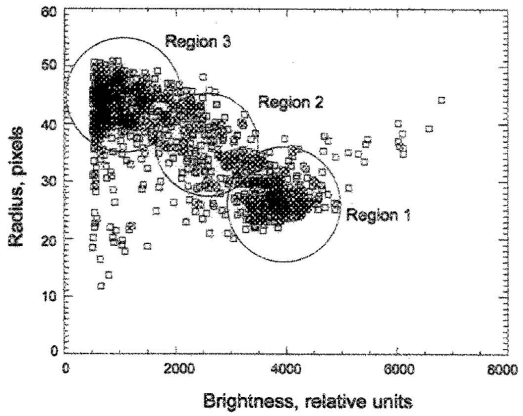

Fig. 3. Distribution of the radius of the Te inclusions (the objects) versus their brightness. Region 1 represents objects of small radius and high brightness; region 3 groups objects with large radius and low brightness, and finally, region 2, between regions 1 and 3 contains objects with medium size and medium brightness.

The algorithm discards Te inclusions that are out of focus and counts only those in focus. This requires two steps. First, a cutoff is applied on brightness to suppress the contribution of objects of low brightness (Te inclusions out of focus) on the negative, i.e., Te inclusions in region 3 (Fig. 3) are discarded. The second step is where the algorithm selects only one of the Te inclusions present at the same position in 3-5 different layers (the number depending on the DOF). For clarity, we use layer instead of image here. The same Te inclusion can appear in several neighboring layers (i.e. in both regions 1 and 2), but would be in focus only in one layer, or at least there would be a layer where that inclusion is in better focus than in the others. The algorithm selects the one in focus, and corrects for shifts of images. In this way, the algorithm ensures that we count each Te inclusion only once. Then, by taking into account the FOV and the size of the z-scan step, the measured number of Te inclusions for each layer can be renormalized per cm^3. For each CZT sample, five different measurements were taken at five different locations over the crystal's length from two perpendicular directions. Their average gives the concentration per cm^3.

By comparing with the high-magnification microscope measurements, we estimated that for the large, >3 μm, inclusions the error in the size determination is ~1 μm. Below 3 μm, the measurements are limited by the small focus depth, ~1.6 μm at 20x magnification. Even though the optical system can locate and count the inclusions with the diameters as small as 0.5 μm, it cannot accurately determine their sizes if their actual diameter <3 μm.

III. Results and Discussion

It is well established, based on the direct measurements carried out with the highly collimated X-ray beam [6,7], that each Te inclusion traps significant amount of charge from an electron cloud. If we consider the Te inclusions to be nontransparent to the electrons, one can easily simulate their effects on the charge collection in CZT devices. The simulations very accurately reproduce the experimental results obtained from the x-ray scans of thin, <2 mm, planar detectors and predicted the cumulative effect of randomly distributed inclusions on the performance of the thick (long-drift) detectors like, e.g., Frisch-ring or pixel devices. First of all, the inclusions reduce the total amount of the collected charge proportionally to the electron cloud drift distances in a same manner as ordinary traps associated with point defects do. This charge loss can be corrected to preserve good energy resolution. Secondly, because they can trap a large number of electrons per interaction with electron clouds, inclusions cause large fluctuations in the collected charge as predicted by the model [8].

Our qualitative measurements taken with ~ 20 Frisch-ring detectors (more than 20 detectors have been tested by now) consistently demonstrate that the samples with higher concentration or larger size Te inclusions showed poorer spectral responses. Furthermore, the correlation between their size and concentration and device's energy resolution becomes more pronounced for thick samples. To provide a quantitative evidence of such correlation, we selected five CZT detectors and accurately evaluated the size distributions and concentrations of Te inclusions. We particularly chose the samples that provided decent spectral responses and had a close to uniform distribution of inclusions. The latter is important to minimize variations of the collected charge related to non-uniform distribution of inclusions.

Table 2 summarizes the results obtained from the selected detectors, which represent different performance quality. In the case of D1, D2 and D3 detectors, the measurements were taken at 5x magnification. For the detectors D4 and D5, a 20x magnification was used. A quick glance at the table suggests that CZT crystals with a high concentration of Te inclusions of ~10 μm in size perform worse than crystals with lower concentrations of similar size inclusions. On the other hand, crystals with small-size Te inclusions, of about 1 μm, and a high concentration of Te inclusions, of ~10^6, can give the same or better energy resolution than crystals with larger Te inclusions and lower concentrations per cm^3. These results are in a good agreement with the simulations of the cumulative effect of Te inclusions in thick detectors [8,9].

TABLE II
Concentration and Size of Te Inclusions, and Energy Resolution Measured for Five CZT Crystals

Detector number	Dimensions, mm	Concentration, cm^{-3}	Diameter range, μm	Resolution, % FWHM at 662 keV
1	6x6x12	$1.0x10^5$	3-20	6.2
2	6x6x12	$9.6x10^4$	3-10	3.8
3	5x6x11	$5.0x10^4$	3-10	1.2
4	5x5x14	$2.7x10^6$	<3	1.4
5	4x4x11	$1.2x10^6$	<3	0.8

Figs. 4-7 show pulse-height spectra, representative IR images and size distribution of Te inclusions measured for the five samples listed in Table 2.

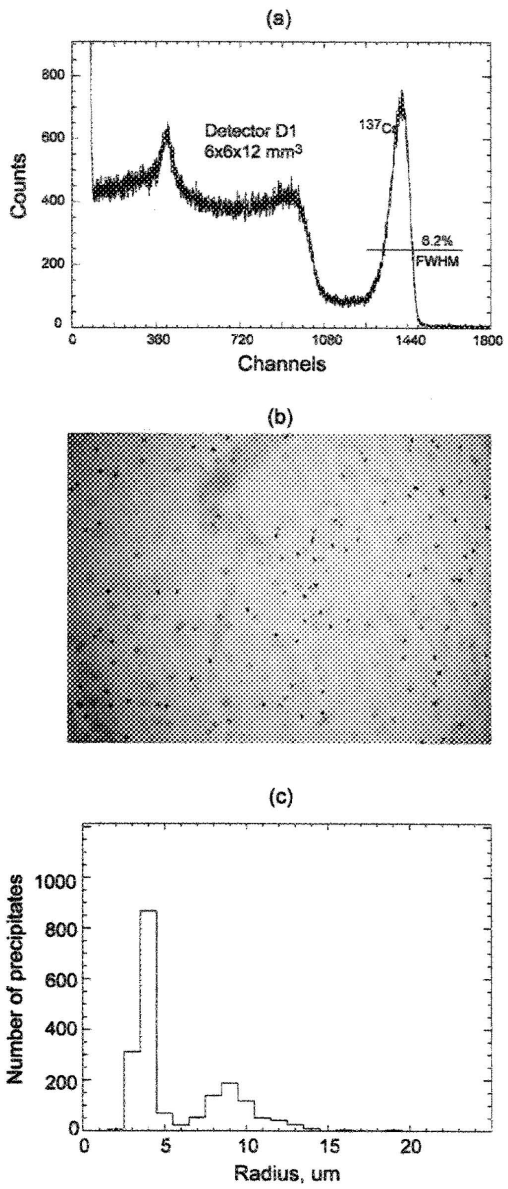

Fig. 4. Results obtained for the sample D1: (a) a pulse-height spectrum, (b) a representative IR image (at 5x magnification) and (c) size distribution of Te inclusions averaged over several measurements. The total inclusions concentration is 1.0×10^5 cm^{-3}. Note, the sample has high concentration of large, >5 μm, inclusions resulting in energy resolution of 6.2%.

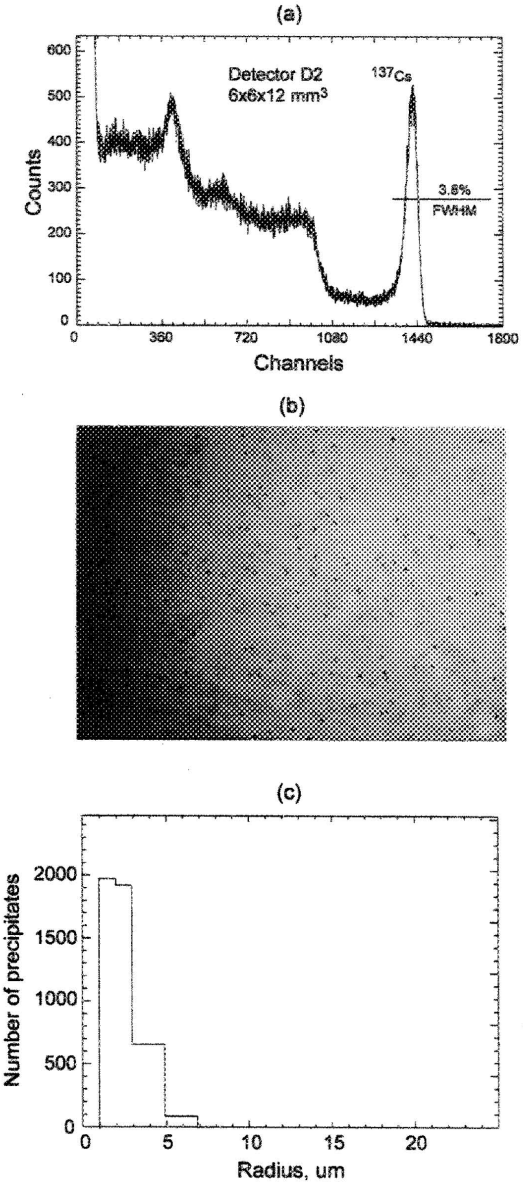

Fig. 5. Results obtained for the sample D2: (a) a pulse-height spectrum, (b) a representative IR image (at 5x magnification) and (c) size distribution of Te inclusions averaged over several measurements. The total inclusions concentration is 9.6×10^4 cm^{-3}. In comparison to D1, D2 has a lower concentration of inclusions with radii of >5 μm, resulting in a better energy resolution of 3.8% FWHM at 662 keV.

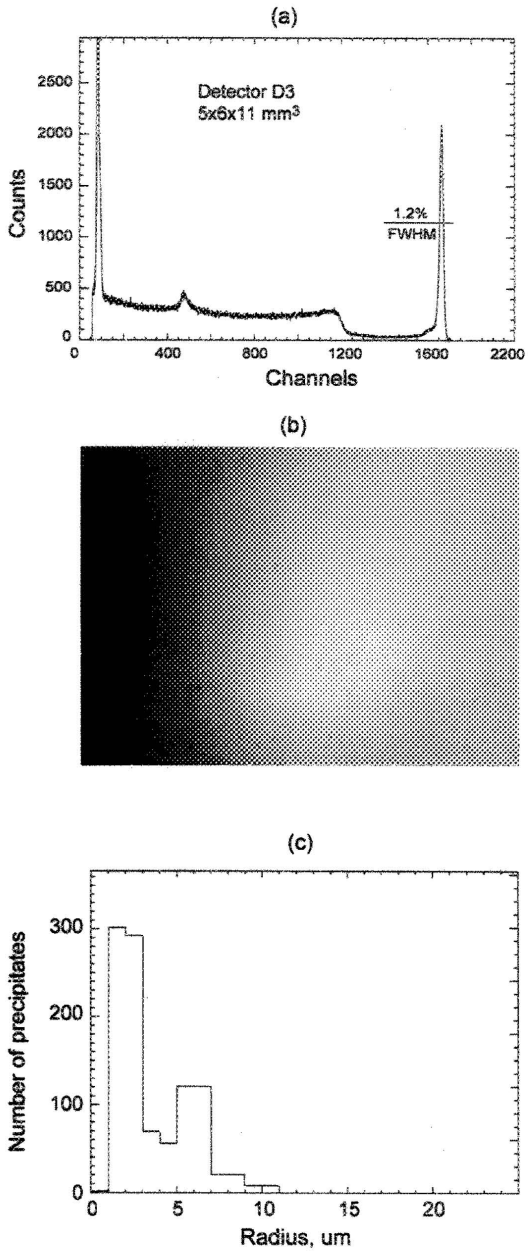

Fig. 6. Results obtained for the sample D3: (a) a pulse-height spectrum, (b) a representative IR image (at 5x magnification) and (c) size distribution of Te inclusions averaged over several measurements. The total inclusions concentration is $5.0x10^4$ cm^{-3}. Note, that D3 has a similar size distribution to that of detector D2 but at a lower concentration of about half of the concentration of detectors D1 and D2, resulting in a significantly better resolution of 1.2%.

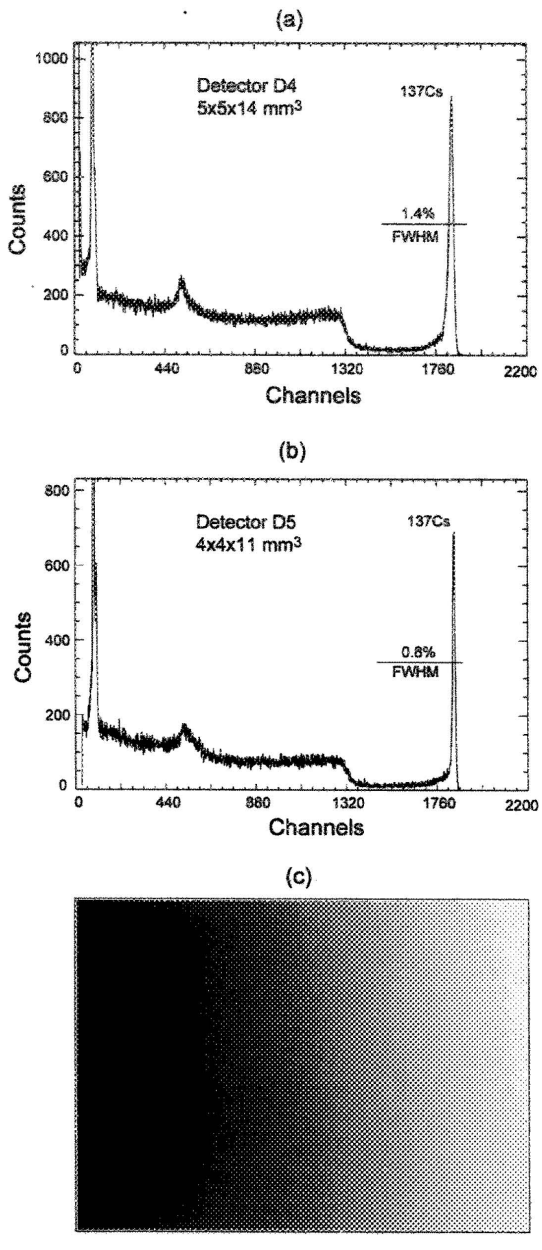

Fig. 7. Results obtained for samples D4 and D5: (a-b) the pulse-height spectra and (c) a representative IR image (at 20x magnification). These samples have only small inclusions of less than 3 μm total concentrations of ~$1.2x10^6$ and $2.7x10^6$ cm^{-3}. Both detectors showed an excellent resolution of 1.2 and 0.8% FWHM at 662 keV.

The detector D1 has high concentration of large (>5 μm) inclusions with a total concentration of $1.0x10^5$ cm^{-3}, resulting in its poor resolution of 6.2% FHWM at 662 keV. The detector D2 has a comparable concentration of $9.6x10^4$ cm^{-3}. However, in contrast to D1, D2 shows a lower concentration of inclusions with diameters of >5 μm, which may explain a slightly better energy resolution of 3.8% FWHM at 662 keV measured for this device. The detector D3 has a similar size distribution to that of detector D2 but at a lower concentration of $5.0x10^4$ cm^{-3}, about half of the concentration of detectors D1 and D2. Correspondently, this device shows significantly better resolution of 1.2%.

The detectors D4 and D5 (fabricated by a different vendor) have only small inclusions of less than 3 μm but with higher concentrations (at ~$1.2x10^6$ cm^{-3} and $2.7x10^6$ cm^{-3}, correspondingly) than samples D1-D3. Both detectors showed an excellent resolution of 0.8 and 1.2%. A slightly higher FWHM of the detector D5 can be attributed to the larger detector thickness.

These results demonstrated that a detector's responses strongly depend on concentration of Te inclusions greater than 5 μm. Below 3 μm, inclusion sizes are very close to the resolution limit of our IR system, the accuracy of which was insufficient to quantitatively measure the correlations between the device's spectral responses, precipitate concentrations, and crystal thicknesses (the etch pit technique would be more appropriate for measuring such small inclusions). Nevertheless, based on these measurements, we can give an upper estimate that still is very important for CZT crystal growers trying to minimize the impact of inclusions in their material. As we showed with IR transmission microscopy, Te inclusions with diameters of <3 μm contribute to the total energy resolution of <1% at 662 keV in CZT detectors of up to 15-mm thick.

IV. Conclusion

In this work, we demonstrated correlations between the size and concentrations of Te inclusions and the spectral response of CZT detectors. It provided the evidence that the Te inclusions, often found in current CZT material, are responsible for degrading the energy resolution of thick CZT detectors. Our experimental results agree well with the predictions given by the model treating Te inclusions as macroscopic areas filled with a high concentration of point traps.

Furthermore, thick CZT detectors made of crystals with a small concentration of small Te inclusions can potentially give the same or better energy resolution than crystals with larger Te inclusions but lower concentrations per cm^3. Also, we observed that CZT crystals with Te inclusions smaller than ~1 μm behave as ordinary traps. Their presence in the material at concentrations lower than 10^6 does not affect significantly the detector's performance, e.g., a FWHM of less than 1% was obtained for 662 keV for the 11-mm long Frisch-ring detector. At high concentrations or in thicker devices, the cumulative effect of small inclusions can be corrected by using a depth-sensing technique. In should be mentioned, however, that the results reported in this article were obtained from a limited number of CZT samples. We expect to validate these results with a higher confidence level as we receive more CZT samples from our vendors.

These results provide an insight into the critical role of the Te inclusions, whose presence in the current CZT material is related to their growth under non-stoichiometric conditions. Hence, these data are very important to the CZT crystal growers because once these defects are understood and can be controlled, large-volume, several cm^3, CZT detectors will become available to users.

Acknowledgment

The United States Government retains, and the publisher, by accepting the article for publication, acknowledges, a world-wide license to publish or reproduce the published form of this manuscript, or allow others to do so, for the United States Government purposes.

References

[1] R. B. James, T. E. Schlesinger, J. C. Lund and M. Schieber, "Cadmium Zinc Telluride Spectrometers for Gamma and X-Ray Applications", in Semiconductors for Room Temperature Nuclear Detector Applications, Vol. 43, edited by R. B. James and T. E. Schlesinger (Academic Press, New York, 1995), p. 334.

[2] C. Szeles and E. E. Eissler, "Current issues of High-pressure Bridgman growth of semi-insulating CdZnTe", in Semiconductors for Room Temperature Radiation Detector Applications II, Vol. 487, edited by R. B. James, T. E. Schlesinger, P. Siffert, W. Dusi, M. R. Squillante, M. O'Connell and M. Cuzin (Materials Research Society, Pittsburgh, PA, 1998), pp. 3-12.

[3] J. R. Heffelfinger, D. L. Medlin, and R. B. James, "Analysis of Grain Boundaries, Twin Boundaries and Te Inclusions in Cadmium Zinc Telluride Grown by High-Pressure Bridgman Method", in Semiconductors for Room Temperature Radiation Detector Applications II, Vol. 487, edited by R. B. James, T. E. Schlesinger, P. Siffert, W. Dusi, M. R. Squillante, M. O'Connell and M. Cuzin (Materials Research Society, Pittsburgh, PA, 1998), p. 33.

[4] C. Szeles, S. E. Cameron, J.-O. Ndap, W. C. Chalmers, "Advances in the crystal growth of semi-insulating CdZnTe for radiation detector applications", *IEEE Trans. Nucl. Sci.*, NS 49, n.5, pp. 2535-2540, 2002.

[5] M. Amman, J. S. Lee, and P. N. Luke, "Electron trapping nonuniformity in high-pressure-Bridgman-grown CdZnTe", *J. Appl. Phys.*, vol. 92, pp. 3198-3206, 2002.

[6] G. A. Carini, A. E. Bolotnikov, G. S. Camarda, G. W. Wright, L. Li, and R. B. James, "Effect of Te inclusions on the performance of CdZnTe detectors", Appl. Phys. Lett. 88, p. 143515, 2006.

[7] G. S. Camarda, A. E. Bolotnikov, G. A. Carini, and R. B. James, "Effects of Tellurium Inclusions on charge collection in CZT Nuclear Radiation Detectors", in Countering Nuclear and Radiological Terrorism, edited by S. Aprkyan and D. Diamond, Springer, 2006, pp. 199-207.

[8] A. E. Bolotnikov, G. S. Camarda, G. A. Carini, Y. Cui, L. Li, and R. B. James, "A. E. Bolotnikov, G. S. Camarda, G. A. Carini, Y. Cui, L. Li, and R. B. James, "Modelling the geometrical effects of Te precipitates on electron transport in CdZnTe", Nucl. Instr. Meth. A 571, pp. 687–698, 2007.

[9] A. E. Bolotnikov, G. S. Camarda, G. A. Carini, Y. Cui, K. T. Kohman, L. Li, M. B. Salomon, and R. B. James, "Performance-limiting Defects in CdZnTe Detectors", submitted to *IEEE Trans. Nucl. Sci.*, 2007.

[10] P. Rudolph, Non-stoichiometry related defects at the melt growth of semiconductor compound crystals – a review", Cryst. Res. Technol. Vol. 38, n. 7-8, pp. 542-554, 2003.

[11] W. J. McNeil, D. S. McGregor, A. E. Bolotnikov, G. W. Wright and R. B. James, "Single-Charge-Carrier-Type Sensing with an Insulating

Frisch Ring CdZnTe Semiconductor Radiation Detector", Appl. Phys. Lett. 84, pp. 1988-1990, 2004.

[12] A. E. Bolotnikov, G. C. Camarda, G. A. Carini, M. Fiederle, L. Li, D. S. McGregor, W. McNeil, G. W. Wright, and R. B. James, "Performance Characteristics of Frisch-Grid CdZnTe Detectors", *IEEE Transactions on Nuclear Science*, NS 53, n.2, pp. 607-614, 2006.

[13] J. C. Crocker and D. G. Grier, "Methods of digital video microscopy for colloidal studies", J. Colloid Interface Sci., Vol. 179, pp. 298-310, 1996.